

HIGH-RESOLUTION OBSERVATIONS OF COMPACT RADIO SOURCES AT 6 AND 18 CENTIMETERS

K. I. KELLERMANN

National Radio Astronomy Observatory,* Green Bank, West Virginia, and Owens Valley
 Radio Observatory,† California Institute of Technology, Pasadena, California

D. L. JAUNCEY‡

Cornell-Sydney University Astronomy Center,§ Cornell University, Ithaca, New York

M. H. COHEN AND B. B. SHAFFER

Owens Valley Radio Observatory,† California Institute of Technology, Pasadena, California

B. G. CLARK AND J. BRODERICK

National Radio Astronomy Observatory,* Green Bank, West Virginia

B. RÖNNÄNG AND O. E. H. RYDBECK

Onsala Space Observatory,# Chalmers Institute of Technology, Gothenburg, Sweden

L. MATVEYENKO

Institute for Space Research, Moscow, U.S.S.R.

I. MOISEYEV

Crimean Astrophysical Observatory, Crimea, U.S.S.R.

V. V. VITKEVITCH

Lebedev Physical Institute, Moscow, U.S.S.R.

AND

B. F. C. COOPER AND R. BATCHELOR

CSIRO Radiophysics Laboratory, Epping, N.S.W., Australia

Received 1971 April 26

ABSTRACT

The small-scale structure of extragalactic radio sources has been studied at 18 and 6 cm wavelengths by using a tape-recording interferometer. At the longest antenna spacing, 10536 km, the baseline at 6 cm was 176 million wavelengths and the resolution was about $0''.0004$ for the stronger sources.

Many sources, including optically identified galaxies and QSOs, are found to have several distinct components of widely differing size in the range from a few hundredths of a second of arc to the limit of our resolution. In general, the smallest components are strongest at the shortest wavelengths, and the dimensions are in good agreement with those expected if the low-frequency cutoffs are due to synchrotron self-absorption. The magnetic field strengths deduced from our observations and the self-absorption cutoff frequency are typically of the order of 10^{-4} gauss. The maximum brightness temperatures observed are 10^{11} °– 10^{12} ° K.

Many sources, including 0106+01, 3C 273, 3C 279, 1555+00, 2145+06, 3C 446, 3C 454.3, and 2345–16 all contain components which are unresolved on the longest baseline and are less than $0''.0004$

* Operated by Associated Universities, Inc., under contract with the National Science Foundation.

† Supported by ONR contract N 00014-67-A-0094-0008.

‡ Supported by NSF grant GP 13950.

§ Supported by NSF grant GP 4262.

|| Supported by AFOSR grant AFOSR-69-1684.

Supported jointly by the Swedish National Science Research Council and the Swedish Council for Applied Research.

in diameter. Observations at shorter wavelengths are required to resolve these sources. Because the maximum brightness temperature is limited to 10^{12} °K by inverse Compton scattering, baselines no greater than the diameter of the Earth are probably adequate to resolve all of the stronger extragalactic sources.

One source, 3C 84, has shown an apparent increase in angular size of about 35 percent in one year.

I. INTRODUCTION

We have previously reported long-baseline interferometer measurements of compact extragalactic radio sources made near 50, 18, 13, 6, and 3 cm wavelengths with resolutions up to about $0''.001$ (Clark *et al.* 1968*a, b*; Kellermann *et al.* 1968, 1970; Jauncey *et al.* 1970; Broderick *et al.* 1970*a, b*). These experiments have shown that angular structure exists in many QSOs and radio galaxies on scales of one thousandth to a few hundredths of an arc second.

This paper presents data obtained in two series of observations made in 1967 April at 18 cm between Lincoln Laboratory in Massachusetts and Green Bank, West Virginia, and during 1969 at 18 and 6 cm using stations in Green Bank and California in the United States, and in Sweden, Australia, and the U.S.S.R. The highest resolution obtained was between Owens Valley, California, and Parkes, Australia, at 6 cm where the baseline was 10536 km or 176 million wavelengths long. Sources larger than 4×10^{-4} arc seconds were resolved on this baseline, which is greater than 80 percent of the Earth's diameter.

The new data have been combined with the previously published material to determine in more detail the small-scale radio structure over a wide range of wavelength, and also to estimate, where possible, the spectra of the individual components within the compact sources. The sources studied include identified QSOs and radio galaxies as well as some unidentified sources.

The observational details are described in § II of this paper. The observed fringe visibilities are tabulated in § III, and the structure of the individual sources is given in § IV. The observations of variable sources are described in § V, and all the results are discussed further in § VI.

II. OBSERVATIONS

All of the observations were made by using the digital tape-recording system developed at the National Radio Astronomy Observatory (Bare *et al.* 1967). Three of these units are in operation. One of the units was used in Green Bank while a second one has been used in Sweden, the Soviet Union, and Australia. The third unit was used at the Lincoln Laboratory and at the Owens Valley Radio Observatory.

A description of the instrumentation, and of the observing and reduction procedures, has been given previously (Clark *et al.* 1968*a*). Standard computer-tape drives were used at each station to record digitally with one-bit samples the signal in a 330-kHz band. Atomic frequency standards were used to synchronize the data recording and to provide a coherent local oscillator signal at each station. Hydrogen masers were used at Green Bank and Lincoln Laboratory as time and frequency standards, while portable rubidium vapor standards were used at all of the other locations (and on a few occasions at Green Bank).

Initial clock synchronization was achieved by receiving the time signals from one or more Loran C navigational stations or by direct comparison with a clock which had previously been compared with the master clock at the U.S. Naval Observatory. In the latter case, the Loran signals or WWVL were still used whenever possible to monitor the time.

The local oscillator frequency at each antenna was derived by using the atomic frequency standard to control a frequency synthesizer. The output of the synthesizer was

then amplified and multiplied to 18 cm. For operation at 6 cm, the 18-cm signal was further multiplied in the front end box. Two different arrangements were used. At Green Bank, a Hewlett Packard Model 5105A synthesizer was operated near 272 MHz, multiplied by 6, and amplified. This is the standard local oscillator system commonly in use at NRAO for spectral-line observations, except that the frequency synthesizer was controlled by an atomic standard. At the other stations a Rhode and Schwartz XUC synthesizer was operated at 820 MHz, amplified, and multiplied by 2. For operation at 18 cm (1670 MHz) the local oscillator frequency was 1640 MHz, and a 30-MHz intermediate frequency was used. For operation at 6 cm (5010 MHz), a multiplier was used to obtain a local oscillator signal at 4860 or 4980 MHz, and the intermediate frequency was either 150 or 30 MHz. In the former case a second local oscillator at 120 MHz, also locked to the atomic standard, was then used to convert to 30 MHz. The 30-MHz intermediate-frequency signal in both cases was then converted in two stages to the range 20–350 kHz, clipped, and sampled at a 720-kHz rate.

Observations were made by using various combinations of stations as shown in Table 1. Where possible, the data were obtained over a range of hour angles to vary the length and direction of the projected baseline. On the longer baselines, however, the requirement of common visibility at reasonable elevations required the observations at the lower declinations to be made only near the interferometer meridian. Most of the observations were made by using only two stations simultaneously, although a three-station experiment was carried out between Green Bank, Owens Valley, and Onsala at 6 cm (1969 January-February).

On each of the baselines we generally observed for from one to three days. Typically we ran from 75 to 100 tape pairs each day at intervals of about 15 minutes, often recording two tapes in succession on each source. Each tape is sufficient to record about 3 minutes of data. For each series of observations, the starting time of each tape was scheduled in advance, although from time to time technical difficulties required minor last-minute modifications to the schedule. Communication between observing sites was usually done by telephone or by teletype machines. Commercial telegraph facilities were also used between the U.S.S.R. and Green Bank.

The observations are summarized in Table 1, which lists all of the baselines which

TABLE 1
INTERFEROMETER BASELINES

Baseline*	λ (cm)	Separation (km)	Separation ($10^6 \lambda$)	Dates
(1)	(2)	(3)	(4)	(5)
GB-HSK, GB-MS..	18	845	4.7	1967 July and August, 1968 April
GB-HC.....	18	3500	19.4	1967 August
GB-ONS.....	18	6319	35.1	1968 January I, 1969 April II
GB-ONS.....	6	6319	105	1968 February I, 1969 January II
GB-OVRO.....	6	3324	55.5	1969 January, March, April, May
OVRO-ONS.....	6	7914	132	1969 February
OVRO-PKS.....	6	10536	176	1969 April
GB-CAO.....	6	8035	134	1969 October

* GB = Green Bank; HSK = Haystack; MS = Millstone; HC = Hat Creek; ONS = Onsala; OVRO = Owens Valley Radio Observatory; PKS = Parkes; CAO = Crimean Astrophysical Observatory.

gave results. Not listed are attempted observations made between Green Bank and Parkes at 6 and 18 cm, and between Parkes and OVRO at 18 cm. Column (1) identifies the two stations, column (2) gives the wavelength, column (3) the antenna separation in kilometers, column (4) the baseline length in wavelengths, and column (5) the dates of the observations. For completeness Table 1 includes the earlier measurements at 6 and 18 cm which have already been published.

a) *Instrumentation*

The instrumentation used at each station is described below.

i) *Green Bank (GB)*

The observations at Green Bank were made by using the 140-foot (42 m) antenna. The 18-cm receiver used a room-temperature nondegenerate parametric amplifier as the first stage with an overall system noise temperature near 200° K. At 6 cm a two-stage nondegenerate cooled parametric amplifier was used, giving a system temperature of about 110° K.

As a local oscillator reference and time standard, we used either a Varian H-10 hydrogen maser on loan from the NASA Goddard Space Flight Center or a Hewlett Packard HP 5065 rubidium vapor standard.

Time at Green Bank was established by receiving the Loran C transmissions from the station at Cape Fear in North Carolina, which was monitored throughout each observing period.

ii) *Lincoln Laboratory, Haystack (HSK) and Millstone (MS)*

The early 18-cm observations from Lincoln Laboratory were made by using the 120-foot (37 m) Haystack antenna (Clark *et al.* 1968a). The new observations were made in 1967 April using the 84-foot (25.6 m) Millstone Hill reflector. A room-temperature nondegenerate parametric amplifier was used, to give an overall system noise temperature of 200° K. As a time and frequency standard, we used the Lincoln Laboratory hydrogen maser which is kept in continuous operation. In addition, the time was checked by monitoring the Loran transmission from Cape Fear, North Carolina.

iii) *Owens Valley Radio Observatory (OVRO)*

The observations at OVRO used the 130-foot (40 m) antenna. Nondegenerate room-temperature parametric amplifiers were used as the first stage at both 6 and 18 cm with overall system noise of 150° and 250° K, respectively. Time was established by comparing a portable rubidium-controlled clock with clocks at the Timing Center at Point Mugu, California, or at the NASA Deep Space Network Station at Goldstone, California, both of which had been directly compared with the U.S. Naval Observatory clock.

iv) *Parkes, Australia (PKS)*

The observations from Australia were made by using the 210-foot (65 m) antenna at the Australian National Radio Astronomy Observatory near Parkes. The 6-cm receiver was a portable unit constructed at the NRAO especially for used at remote sites and gave a system temperature of 130° K. This receiver, including parametric amplifier, mixer, radiofrequency amplifier, power supplies, and multiplier for the local oscillator chain, was housed in a small temperature-controlled box that was mounted directly at the focus.

Time in Australia was synchronized with the time in Owens Valley via the NASA tracking stations at Tidbinbilla, Australia, and Goldstone, California. The tracking stations themselves were synchronized to an accuracy of a few microseconds by the transmission of a radar signal from Goldstone to Tidbinbilla via the Moon.

v) *Onsala Space Observatory, Sweden (ONS)*

The observations from Sweden were made by using the 84-foot (25.6 m) telescope at the Onsala Space Observatory near Gothenburg. Both the 6 and 18 cm receivers used a rutile traveling-wave maser as a low-noise preamplifier, and the total system noise temperature was less than 50° K at both wavelengths. Maser amplifiers are particularly suitable for long-baseline interferometry where the bandwidths and integration times are restricted by available recording facilities so that the lowest-noise receivers are important. The use of the maser preamplifier at 6 cm during the 1969 observations improved the sensitivity by a factor of about 2.5 over that obtained in the earlier observations (Kellermann *et al.* 1968).

Time in Sweden was obtained from a cesium clock located at the Research Institute for National Defense in Stockholm. The cesium clock in Stockholm had been previously compared with the U.S. Naval Observatory master clock via a flying clock experiment conducted by the USNO. The time at Onsala was further checked by monitoring the Loran C transmission from the Ejde station of the Norwegian Sea chain.

vi) *Crimean Astrophysical Observatory, U.S.S.R. (CAO)*

The observations from the U.S.S.R. were made by using the 22-m precision radio telescope of the Crimean Astrophysical Observatory located near Simeis. The 6-cm portable receiver used at Parkes was also used on the Crimean telescope.

Synchronization of time between Green Bank and Crimea was achieved by flying the Onsala rubidium clock from Stockholm, Sweden, to Crimea via Leningrad. The time in Crimea was monitored by receiving the Loran C transmission from the Mediterranean Sea chain station in Turkey, which had been synchronized to the U.S. Naval Observatory master clock in Washington immediately prior to our experiment. A preliminary account of this experiment has already been published (Broderick *et al.* 1970a, b).

b) *Data Analysis*

The natural interference-fringe rate varied from several hundred hertz to several kilohertz on the longer baselines. Since the fringe-reduction program averaged the data for a period of 0.4 ms, only fringe rates less than a few hundred hertz could be analyzed. During the first few series of observations, the frequency of the local oscillator at one station was offset by a small amount to reduce the fringe frequency to a few hertz. This procedure proved inconvenient for two reasons. First, it was necessary to calculate in advance the local oscillator settings, so that it was difficult to make last-minute modifications to the program. Second, it was necessary to change the synthesizer frequency often, and this provided many opportunities for operator error.

For some of the later observations, therefore, we kept the local oscillator frequencies fixed at both ends of the baseline, so that the interference fringes were at their natural rate, and the fringe-reduction program was modified to multiply the data by a square wave of the expected fringe frequency, before multiplying the two data sets together.

The analysis of the tape pairs was done with the NRAO IBM 360/50, the Caltech 360/75, or the 360/91 at the Goddard Space Flight Center. Typically, a range of fringe frequency of ± 0.3 Hz and a delay range of ± 5 μ s were searched. The reduction took about 70, 10, and 5 minutes, respectively, in the three machines for a single 3-minute tape pair.

In general, somewhat less than one-half of the tape pairs showed fringes. In some cases the absence of fringes is no doubt due to the resolution of the source. Sometimes, however, when several pairs of tapes were run on the same source at similar hour angles, one or more pairs did not show fringes. Usually, but not always, when fringes were seen, the amplitudes of separate pairs agreed within the limits of error expected from the

interferometer sensitivity. The reasons for the absence of fringes on some tape pairs, or discrepancies between pairs, are not fully understood, although some cases may be explained by possible operator error in setting the synthesizer frequency, in pointing the antenna, errors in the data sampling, or by instabilities in the atomic frequency standard.

We have therefore rejected all tape pairs which did not show fringes. This procedure, however, results in a systematic overestimate of fringe amplitude for those sources near the limit of detection.

c) Calibration of Fringe Amplitudes

One of the major uncertainties in interpreting the data is the difficulty in calibrating the interferometer sensitivity, particularly at the longer baselines where there are no sources which *a priori* are known to be unresolved. Furthermore, the different baselines give little or no overlap in the (u, v) -plane, and the flux density of the sources may vary between the observing periods, so that even the calibration of the relative fringe amplitudes among the different baselines is often difficult.

The calibration of the Millstone-Green Bank baseline at 18 cm is straightforward and is based on the sources CTA 102 and CTD 93, which previous measurements (Kellermann *et al.* 1968) indicated should be unresolved on this baseline. The Green Bank-Owens Valley baseline at 18 cm was calibrated by using 3C 279, which had been previously observed over a similar baseline (Clark *et al.* 1968*b*).

At 6 cm the calibration is less direct. The sensitivity of the different baselines was roughly estimated from knowledge of the gain and system temperature of the individual antenna systems which, unfortunately, were not always accurately measured. In this way four sources, 0106+01, 4C 39.25, 1555+00, and 2145+06 were found to have components which were essentially unresolved out to the longest spacing at which they were observed. The strongest of these, 4C 39.25, is not visible from Parkes and thus could be observed only out to 135 million wavelengths. At least two of these four sources were observed on each baseline at 6 cm and were used to tie together the data from different baselines. Moreover, there were a number of other sources common to the three sets of Green Bank-OVRO observations that could be used to normalize these observations. Fortunately, these sources showed little variation in total flux density during the time of the observations.

The scale of fringe amplitude was determined by estimating the unresolved flux density of the above four sources from consideration of their spectra and from previous observations at 13 cm made with comparable resolution.

Since the fringe visibility cannot exceed unity, we estimate that the results in Tables 2 and 3 are not systematically low by more than 15 percent, and we believe that they are not too high by more than 20 percent.

In addition to the calibration uncertainty described above, other errors in the quoted fringe visibilities are due to receiver noise; and to uncertainties in the determination of the total system temperature and in the antenna temperature of each source. Errors in the latter were introduced by uncertainties in the pointing of the individual antennas and to uncertainties in the gain changes caused by structural deformations at the extreme hour angles where many of the observations were made. Since unswitched total power receivers were used for most of these observations, it was difficult to measure accurately the antenna temperature of each source or to check the pointing.

III. FRINGE AMPLITUDES

The results of all the observations are shown in Table 2 for the 18-cm data and in Table 3 for the 6-cm data.

In both tables, column (1) gives the source name; column (2) the total flux density at the time of observation, column (3) the observed fringe amplitude, and columns (4) and

TABLE 2—Continued

Source (1)	S_t (2)	S_e (3)	d (4)	θ (5)	γ (6)	Baseline (7)
4C 39.25.....	3.0	1.8±0.9	15.3	52	0.60±0.30	GB-OVRO
		1.2±0.9	17.2	69	0.40±0.30	GB-OVRO
		1.1±0.9	16.1	60	0.37±0.30	GB-OVRO
1055+01.....	3.2	2.4±0.8	3.1	47	0.75±0.25	GB-HSK
		1.7±1.0	3.7	59	0.53±0.31	GB-MS
		1.1±1.0	4.5	65	0.34±0.31	GB-MS
		1.5±0.9	8.3	83	0.47±0.28	GB-OVRO
1127-14.....	6.4	7.3±1.2	4.2	69	1.14±0.19	GB-HSK
		4.2±1.0	12.1	104	0.66±0.16	GB-OVRO
		4.0±1.0	13.5	73	0.63±0.16	GB-OVRO
		3.7±0.8	19.5	94	0.58±0.13	GB-HC
		2.4±0.5	35.0	73	0.38±0.08	GB-ONS
1148-00.....	3.2	3.3±0.8	3.4	55	1.03±0.25	GB-HSK
		3.4±0.8	4.6	65	1.06±0.25	GB-HSK
		1.5±0.9	8.3	83	0.47±0.27	GB-OVRO
		1.7±0.9	13.5	86	0.53±0.27	GB-OVRO
(3C 273).....	29	29.0±3.0	2.2	19	1.00±0.10	GB-MS
		24.5±2.6	2.6	36	0.85±0.09	GB-HSK
		22.7±2.5	3.9	58	0.78±0.09	GB-HSK
		20.0±2.2	4.2	61	0.69±0.08	GB-HSK
		18.8±2.1	4.2	63	0.65±0.07	GB-HSK
		18.5±2.1	4.3	62	0.64±0.07	GB-HSK
		20.5±2.2	4.5	64	0.71±0.08	GB-HSK
		21.4±2.3	4.5	65	0.74±0.08	GB-MS
		16.8±1.9	4.6	65	0.58±0.07	GB-HSK
		18.8±2.1	4.7	65	0.65±0.07	GB-HSK
		15.6±1.8	8.3	103	0.54±0.06	GB-HC
		8.6±1.4	10.3	83	0.30±0.05	GB-OVRO
		13.0±1.6	13.4	92	0.45±0.06	GB-HC
		13.9±1.7	19.3	94	0.48±0.06	GB-HC
		14.5±1.8	19.3	94	0.50±0.06	GB-HC
		10.0±2.0	27.0	74	0.35±0.07	GB-ONS I
		8.4±1.7	34.0	77	0.29±0.06	GB-ONS I
3C 279.....	11	9.0±1.1	3.8	64	0.82±0.10	GB-HSK
		7.6±1.1	4.3	65	0.69±0.10	GB-HSK
		8.9±1.1	4.5	66	0.81±0.10	GB-HSK
		6.6±1.1	4.7	65	0.60±0.10	GB-HSK
		5.0±1.0	9.7	87	0.45±0.09	GB-HC
		5.5±1.0	14.3	100	0.50±0.09	GB-HC
		5.5±1.1	17.5	90	0.50±0.10	GB-OVRO
		3.6±1.0	19.4	93	0.33±0.09	GB-HC
		5.7±1.0	19.5	93	0.52±0.09	GB-HC
		5.7±1.2	28.2	74	0.52±0.11	GB-ONS I
		6.3±1.3	34.4	77	0.57±0.12	GB-ONS I
1245-19.....	4.4	4.3±1.0	1.4	71	0.98±0.23	GB-MS II
		3.6±1.0	1.7	86	0.58±0.16	GB-MS II
3C 287.....	6.2	1.9±1.0	3.0	81	0.31±0.16	GB-MS II
		2.4±0.8	4.5	50	0.39±0.13	GB-HSK
		2.7±0.8	4.6	53	0.44±0.13	GB-HSK
		2.7±0.8	4.7	65	0.44±0.13	GB-HSK
		10.2±1.3	1.8	170	0.75±0.10	GB-HSK
3C 286.....	13.5	4.3±0.8	3.7	9	0.32±0.06	GB-HSK
		5.4±0.9	4.2	141	0.40±0.07	GB-HSK
		3.4±0.8	4.6	53	0.25±0.06	GB-HSK
		3.8±0.8	4.7	64	0.28±0.06	GB-HSK
		7.0±1.3	4.3	60	0.93±0.17	GB-HSK
		1.2±0.9	18.5	79	0.19±0.12	GB-OVRO
DA 406.....	3.2	1.6±0.9	16.6	66	0.50±0.28	GB-OVRO
		3.1±0.8	4.5	63	0.94±0.24	GB-HSK
1510-08.....	3.3	3.0±1.0	16.0	93	0.91±0.30	GB-OVRO

TABLE 2
18-CENTIMETER VISIBILITIES

Source (1)	S_t (2)	S_e (3)	d (4)	θ (5)	γ (6)	Baseline (7)
0019-00.....	2.6	2.2±1.0	3.1	62	0.85±0.39	GB-MS
		2.1±1.0	4.2	51	0.81±0.39	GB-MS
NRAO 91.....	3.3	2.4±1.0	3.5	74	0.73±0.30	GB-MS
		2.1±0.8	4.0	48	0.64±0.23	GB-HSK
CTA 21.....	7.0	1.8±1.0	4.7	63	0.55±0.30	GB-MS
		6.2±1.1	3.4	29	0.89±0.16	GB-HSK
		5.7±1.1	3.5	33	0.82±0.16	GB-MS
		5.7±0.9	4.0	71	0.82±0.12	GB-HSK
		5.9±0.9	4.6	61	0.84±0.12	GB-HSK
		4.9±0.9	4.7	62	0.70±0.12	GB-HSK
		2.6±1.0	15.2	81	0.37±0.14	GB-HC
		1.6±0.4	34.0	77	0.23±0.06	GB-ONS I
3C 84.....	11.0	5.9±1.1	1.5	146	0.54±0.10	GB-MS
		5.8±1.1	2.0	124	0.53±0.10	GB-MS
		6.2±1.1	2.4	66	0.56±0.10	GB-MS
		5.4±1.1	4.0	84	0.49±0.10	GB-MS
		3.1±1.0	4.3	171	0.28±0.09	GB-HSK
		4.8±1.1	4.7	55	0.44±0.09	GB-MS
		4.1±1.0	4.7	58	0.37±0.09	GB-HSK
		1.8±0.4	33.2	128	0.16±0.04	GB-ONS II
		2.0±0.4	34.3	142	0.18±0.04	GB-ONS II
		3.5±0.9	4.3	75	1.10±0.28	GB-HSK
NRAO 140.....	3.2	2.9±0.9	4.1	160	0.91±0.28	GB-HSK
		3.7±0.9	4.5	176	0.93±0.22	GB-HSK
NRAO 150.....	4.0	2.1±1.0	1.4	139	0.28±0.13	GB-MS
		2.9±1.0	2.0	125	0.39±0.13	GB-MS
3C 119.....	7.5	2.9±1.0	2.5	110	0.39±0.13	GB-MS
		4.1±1.0	4.1	81	0.55±0.13	GB-MS
		3.4±0.9	4.3	3	0.45±0.12	GB-HSK
		1.4±0.9	17.4	79	0.19±0.12	GB-OVRO
		1.0±0.9	9.1	89	0.76±0.45	GB-OVRO
		2.8±1.1	4.6	58	0.93±0.37	GB-MS
		2.6±0.8	2.4	165	0.65±0.20	GB-HSK
0420-01.....	2.1	3.7±1.0	3.9	55	0.92±0.25	GB-HSK
		3.0±0.9	7.6	76	0.42±0.13	GB-OVRO
		2.8±0.9	10.8	78	0.40±0.13	GB-OVRO
		1.9±0.4	34.0	74	0.31±0.06	GB-ONS I
		1.6±1.0	2.0	68	0.19±0.12	GB-MS
0428+20.....	3.0	4.2±1.0	4.2	62	1.05±0.24	GB-MS
		4.2±1.0	4.2	62	1.05±0.24	GB-MS
3C 120.....	4.0	3.4±1.0	4.6	65	0.81±0.24	GB-MS
		2.3±0.9	9.2	88	0.55±0.22	GB-OVRO
3C 138.....	8.5	2.2±0.9	14.7	88	0.53±0.22	GB-OVRO
		2.2±0.9	14.7	88	0.53±0.22	GB-OVRO
NRAO 190.....	4.0	5.1±1.1	2.1	152	0.25±0.05	GB-MS
		4.0±0.8	2.6	128	0.20±0.04	GB-HSK
3C 147.....	20	3.2±0.8	3.2	106	0.16±0.04	GB-HSK
		3.7±1.0	4.0	88	0.18±0.05	GB-MS
		1.8±1.0	4.1	85	0.09±0.05	GB-MS
		2.4±1.0	4.2	83	0.12±0.05	GB-MS
		2.5±1.0	4.2	82	0.13±0.05	GB-MS
		4.2±0.9	4.5	178	0.21±0.04	GB-HSK
		1.3±1.0	4.7	26	0.60±0.45	GB-MS
		4.3±1.0	4.0	50	1.16±0.27	GB-MS
0607-15.....	2.2	2.5±0.9	7.2	60	0.67±0.24	GB-OVRO
		2.2±0.9	14.3	78	0.59±0.24	GB-OVRO
0742+10.....	3.7	3.9±1.0	1.5	73	1.18±0.30	GB-MS
		3.0±1.0	1.5	73	0.91±0.30	GB-MS
0834-20.....	3.3	2.9±1.0	3.0	75	0.88±0.30	GB-MS
		1.4±0.9	13.2	70	0.42±0.27	GB-OVRO

TABLE 2—*Continued*

Source (1)	S_t (2)	S_e (3)	d (4)	θ (5)	γ (6)	Baseline (7)	
4C 05.64.....	2.5	1.3±0.9	15.8	85	0.52±0.36	GB-OVRO	
		1.8±0.9	16.8	86	0.72±0.36	GB-OVRO	
1555+00.....	1.6	1.2±0.9	15.0	86	0.75±0.56	GB-OVRO	
		1.7±0.9	16.6	66	1.06±0.56	GB-OVRO	
CTD 93.....	4.2	3.4±1.1	2.1	74	0.81±0.26	GB-MS	
		3.9±1.1	4.0	30	0.93±0.26	GB-MS	
		3.5±1.1	4.7	51	0.83±0.26	GB-MS	
		1.6±0.4	35.0	69	0.38±0.09	GB-ONS I	
3C 345.....	6.1	4.9±1.1	2.5	107	0.80±0.18	GB-MS	
		3.9±1.1	4.5	70	0.64±0.18	GB-MS	
		6.5	5.3±0.9	4.7	63	0.81±0.14	GB-HSK
		6.5	1.6±0.4	34.3	80	0.25±0.06	GB-ONS I
NRAO 530.....	5.2	4.7±0.9	4.7	64	0.91±0.17	GB-HSK	
		1.9±0.9	18.0	87	0.37±0.17	GB-OVRO	
3C 380.....	13.0	4.7±1.1	2.1	147	0.36±0.09	GB-MS	
		3.0±0.8	4.0	86	0.23±0.06	GB-HSK	
		3.9±0.9	14.7	21	0.22±0.07	GB-OVRO	
3C 418.....	5.2	3.7±0.8	3.1	115	0.71±0.15	GB-HSK	
		3.7±0.8	4.6	20	0.71±0.15	GB-HSK	
		2127+04.....	3.7	4.8±0.9	4.7	65	1.29±0.24
1.3±0.9	15.0	82		0.35±0.24	GB-OVRO		
2145+06.....	3.0	1.7±0.9	14.4	82	0.57±0.30	GB-OVRO	
VRO 42.22.01...	6.4	4.7±1.0	3.6	78	0.75±0.16	GB-MS	
2203-18.....	6.1	3.5±1.0	1.2	64	0.57±0.16	GB-MS	
		2.5±0.8	2.1	72	0.41±0.13	GB-HSK	
		2.2±1.0	2.7	74	0.36±0.16	GB-MS	
		6.1±1.0	2.9	18	0.96±0.16	GB-HSK	
		6.1±1.0	3.2	33	0.96±0.16	GB-HSK	
		6.6±1.2	4.7	66	1.03±0.19	GB-MS	
		5.5±1.0	10.7	78	0.86±0.16	GB-HSK	
CTA 102.....	6.4	3.9±0.9	17.7	88	0.61±0.14	GB-HSK	
		3.5±0.8	18.6	90	0.55±0.13	GB-HSK	
		4.5±0.9	18.0	89	0.71±0.14	GB-OVRO	
		3.5±0.7	34.8	74	0.55±0.13	GB-ONS I	
		4.1±1.1	1.7	19	0.73±0.20	GB-MS	
		1.9±1.0	2.0	64	0.34±0.18	GB-MS	
		2.1±1.0	4.6	35	0.37±0.18	GB-MS	
3C 446.....	5.6	9.4±1.4	2.6	69	0.73±0.11	GB-MS	
		11.0±1.4	3.2	20	0.86±0.11	GB-HSK	
		10.2±1.4	3.4	28	0.80±0.11	GB-HSK	
		10.0±1.4	4.0	84	0.78±0.11	GB-HSK	
		8.4±1.1	10.5	70	0.66±0.09	GB-HC	
		2.6±0.8	17.8	86	0.20±0.06	GB-HC	
		2.2±0.8	19.5	94	0.17±0.06	GB-HC	
3C 454.3.....	12.8	4.0±0.8	34.6	73	0.31±0.06	GB-ONS I	

(5) the spacing in millions of wavelengths and orientation of the projected baseline. Column (6) gives the fringe visibility γ , and column (7) the location of the ends of the baseline using the abbreviations shown in Table 1.

The errors in fringe amplitudes quoted in Tables 2 and 3 do not include the possible uncertainty in overall calibration. They do include the uncertainty due to noise fluctuations and an estimate of the errors introduced by changes in antenna gain, system temperature, and pointing. Because of the one-bit sampling, the fringe amplitudes are insensitive to changes in receiver gain.

Some of the fringe amplitudes do not greatly exceed the quoted errors, and it might

TABLE 3
6-CENTIMETER VISIBILITIES

Source (1)	S_t (2)	S_e (3)	d (4)	θ (5)	γ (6)	Baseline (7)
0106+01.....	2.4	2.7±1.0	23	83	1.12±0.42	GB-OVRO
	2.5	2.6±1.3	26	83	1.04±0.52	GB-OVRO
	2.5	2.3±1.3	55	89	0.92±0.52	GB-OVRO
	2.7	3.0±0.6	83	72	1.11±0.22	GB-ONS II
	2.7	3.2±0.6	105	77	1.18±0.22	GB-ONS II
	2.4	2.5±0.9	134	87	1.08±0.37	GB-CAO
	2.6	2.3±0.7	169	43	0.88±0.27	OVRO-PKS
	2.6	3.1±0.7	170	43	1.19±0.27	OVRO-PKS
CTA 21.....	3.1	1.4±1.0	58	31	0.45±0.32	GB-OVRO I
3C 84.....	22.0	14.2±1.6	37	157	0.65±0.07	GB-OVRO I
	22.0	12.2±1.7	38	6	0.56±0.08	GB-OVRO
	22.0	10.8±1.7	46	44	0.49±0.08	GB-OVRO
	22.0	8.6±1.6	51	65	0.39±0.07	GB-OVRO
	22.0	2.1±0.5	82	110	0.09±0.02	GB-ONS II
	19.7	6.4±2.2	84	0	0.32±0.11	GB-ONS I
	22.0	1.7±0.5	92	32	0.08±0.02	GB-ONS II
	22.0	2.0±0.5	97	93	0.09±0.02	OVRO-ONS
	22.0	4.0±0.7	127	90	0.18±0.03	OVRO-ONS
	22.0	5.9±0.7	135	85	0.27±0.03	GB-CAO
	NRAO 140.....	2.5	2.1±1.2	41	50	0.84±0.48
CTA 26.....	2.3	2.1±0.5	83	75	0.91±0.21	GB-ONS II
	2.3	2.3±0.7	173	45	1.00±0.30	OVRO-PKS
NRAO 150.....	7.3	4.8±1.2	45	14	0.66±0.16	GB-OVRO
	7.3	2.0±0.5	99	35	0.27±0.07	GB-ONS II
	7.3	2.3±0.5	104	33	0.31±0.07	GB-ONS II
3C 120.....	8.5	4.4±1.2	28	78	0.52±0.14	GB-OVRO
	8.5	2.5±1.2	40	82	0.29±0.14	GB-OVRO
	9.0	6.2±2.1	67	74	0.68±0.23	GB-ONS I
	9.0	4.7±2.0	99	75	0.52±0.22	GB-ONS I
	10.0	1.7±0.5	104	76	0.17±0.05	GB-ONS II
0420-01.....	3.5	1.5±0.7	173	45	0.43±0.20	OVRO-PKS
NRAO 190.....	3.7	3.0±1.0	38	87	0.81±0.27	GB-OVRO
	3.2	1.7±0.7	168	44	0.53±0.21	OVRO-PKS
	3.2	1.9±0.7	170	44	0.59±0.21	OVRO-PKS
0605-08.....	2.7	2.5±0.5	96	79	0.92±0.18	GB-ONS II
	2.7	2.0±0.5	100	79	0.74±0.18	GB-ONS II
0607-15.....	3.0	1.6±1.0	36	106	0.53±0.33	GB-OVRO
0742+10.....	3.5	3.7±1.0	20	57	1.05±0.28	GB-OVRO
	3.5	2.4±0.7	68	55	0.68±0.20	GB-ONS
4C 39.25.....	8.2	8.8±1.4	42	43	1.07±0.17	GB-OVRO
	8.2	7.6±1.1	44	36	0.93±0.13	GB-OVRO
	8.2	5.1±1.4	45	66	0.62±0.17	GB-OVRO
	8.2	5.4±1.4	55	87	0.65±0.17	GB-OVRO
	8.1	7.2±0.9	83	175	0.88±0.12	GB-ONS II
	8.1	6.2±0.9	87	80	0.76±0.12	GB-ONS II
	7.6	6.5±1.5	95	72	0.80±0.18	GB-ONS I
	8.1	5.2±0.7	99	51	0.64±0.09	GB-ONS II
	8.1	7.0±0.7	102	79	0.86±0.09	GB-ONS II
	8.1	6.6±0.7	105	74	0.81±0.09	GB-ONS II
	8.2	6.0±0.8	119	95	0.73±0.10	OVRO-ONS
	8.2	6.8±0.8	119	97	0.83±0.10	OVRO-ONS
	8.6	7.0±0.8	134	89	0.81±0.09	GB-CAO
1055+01.....	2.5	1.6±0.5	89	74	0.64±0.20	GB-ONS II
	4.0	3.3±0.8	133	86	0.82±0.20	GB-CAO
	2.8	2.3±0.7	173	45	0.82±0.25	OVRO-PKS
1127-14.....	2.8	1.5±0.7	173	45	0.54±0.25	OVRO-PKS
	8.2	1.3±0.7	172	48	0.16±0.0	OVRO-PKS
	8.2	1.2±0.7	173	48	0.14±0.08	OVRO-PKS

TABLE 3—Continued

Source (1)	S_l (2)	S_c (3)	d (4)	θ (5)	γ (6)	Baseline (7)	
3C 273*	32.0	25.5±2.5	24	81	0.80±0.08	GB-OVRO	
	32.0	25.8±2.4	24	82	0.81±0.08	GB-OVRO	
	32.0	24.6±2.5	30	83	0.77±0.08	GB-OVRO	
	32.0	5.3±1.1	33	84	0.17±0.03	GB-OVRO	
	32.0	15.3±2.0	43	86	0.48±0.06	GB-OVRO	
	32.0	15.1±1.7	48	86	0.49±0.05	GB-OVRO	
	32.0	14.8±2.0	49	86	0.46±0.06	GB-OVRO	
	32.0	16.0±1.7	49	86	0.50±0.05	GB-OVRO	
	32.0	17.0±1.7	51	87	0.53±0.05	GB-OVRO	
	32.0	12.4±1.6	55	88	0.38±0.05	GB-OVRO	
	30.0	9.8±2.2	74	68	0.33±0.07	GB-ONS I	
	31.0	10.7±1.1	81	71	0.35±0.04	GB-ONS II	
	31.0	8.3±1.1	85	71	0.27±0.04	GB-ONS II	
	30.0	7.0±1.7	104	75	0.23±0.06	GB-ONS I	
	34.0	7.0±1.0	124	87	0.21±0.03	GB-CAO	
	34.0	9.2±1.1	128	86	0.27±0.03	GB-CAO	
	31.0	6.0±1.0	132	79	0.19±0.03	OVRO-ONS	
	34.0	10.9±1.2	133	86	0.32±0.03	GB-CAO	
	34.0	8.7±1.1	133	86	0.29±0.03	GB-CAO	
	32.0	7.4±0.9	172	43	0.23±0.03	OVRO-PKS	
	32.0	6.9±0.9	172	43	0.22±0.03	OVRO-PKS	
	32.0	6.2±0.9	172	45	0.19±0.03	OVRO-PKS	
	32.0	3.3±0.8	175	45	0.10±0.03	OVRO-PKS	
	3C 279.....	16.5	15.1±1.7	27	84	0.92±0.10	GB-OVRO
		16.5	4.8±1.1	40	83	0.29±0.07	GB-OVRO
		16.5	16.8±1.8	45	92	1.02±0.11	GB-OVRO
		16.5	14.0±1.7	50	89	0.84±0.10	GB-OVRO
16.5		13.4±1.8	51	90	0.81±0.11	GB-OVRO	
16.5		8.3±1.3	55	89	0.50±0.08	GB-OVRO	
15.4		5.9±1.6	102	75	0.38±0.10	GB-ONS I	
16.5		7.7±0.9	102	78	0.47±0.05	GB-ONS II	
16.5		4.6±1.0	129	80	0.28±0.06	OVRO-ONS	
16.5		4.2±1.0	130	80	0.25±0.06	OVRO-ONS	
16.5		6.3±1.0	133	86	0.38±0.06	GB-CAO	
16.5		7.1±1.0	134	87	0.43±0.06	GB-CAO	
16.5		5.4±1.0	134	86	0.32±0.06	GB-CAO	
16.5		4.2±0.8	164	45	0.25±0.05	OVRO-PKS	
16.5		4.8±0.8	164	45	0.29±0.05	OVRO-PKS	
16.5		4.9±0.8	168	46	0.30±0.05	OVRO-PKS	
16.5		4.7±0.8	170	46	0.28±0.05	OVRO-PKS	
1510-08.....		2.4	2.0±1.2	55	89	0.83±0.50	GB-OVRO
		2.3	2.3±0.5	92	80	1.00±0.21	GB-ONS II
		2.7	3.2±0.8	134	86	1.18±0.30	GB-CAO
	2.7	3.4±0.8	134	86	1.25±0.29	GB-CAO	
	2.3	1.5±0.7	173	57	0.65±0.30	OVRO-PKS	
4C 05.64.....	2.6	1.6±0.5	104	76	0.62±0.19	GB-ONS II	
1555+00.....	2.2	1.9±1.0	47	88	0.86±0.45	GB-OVRO	
	2.2	2.8±1.0	51	88	1.27±0.45	GB-OVRO	
	2.2	2.1±0.5	81	73	0.95±0.23	GB-ONS II	
	2.2	2.5±0.5	104	77	1.13±0.23	GB-ONS II	
	2.8	3.5±0.8	134	87	1.25±0.29	GB-CAO	
	2.2	2.4±0.7	172	45	1.09±0.32	OVRO-PKS	
	2.2	2.1±0.7	173	45	0.95±0.32	OVRO-PKS	
	2.2	2.3±0.7	174	45	1.05±0.32	OVRO-PKS	
	2.8	3.2±0.5	101	85	1.14±0.15	GB-ONS II	
	3C 345.....	7.9	8.3±1.4	37	13	1.1 ±0.2	GB-OVRO
7.9		8.5±1.4	39	26	1.1 ±0.2	GB-OVRO	
7.9		5.5±1.3	47	55	0.70±0.16	GB-OVRO	
6.5		3.8±1.5	90	135	0.58±0.23	GB-ONS I	
7.9		6.1±0.7	95	45	0.77±0.08	GB-ONS II	

* Exclusive of Component A.

TABLE 3—Continued

Source (1)	S_t (2)	S_c (3)	d (4)	θ (5)	γ (6)	Baseline (7)	
3C 345 (<i>cont.</i>)...	7.9	6.6±0.7	101	86	0.84±0.09	GB-ONS II	
	7.9	5.2±0.6	105	68	0.66±0.09	GB-ONS II	
	8.5	6.4±1.0	116	56	0.75±0.12	GB-CAO	
	7.9	5.5±0.8	117	99	0.70±0.10	OVRO-ONS	
	8.5	3.2±0.9	131	85	0.38±0.11	GB-CAO	
	8.5	4.3±0.9	132	76	0.51±0.11	GB-CAO	
NRAO 530.....	4.2	2.0±1.2	53	92	0.48±0.29	GB-OVRO	
3C 380.....	7.2	2.9±1.2	46	36	0.39±0.17	GB-OVRO	
	7.2	2.5±1.2	48	77	0.35±0.17	GB-OVRO	
	7.2	2.7±1.2	53	69	0.38±0.17	GB-OVRO	
2134+00.....	12.1	3.1±1.0	43	87	0.26±0.08	GB-OVRO	
	12.1	3.3±1.0	52	88	0.27±0.08	GB-OVRO	
	12.1	8.5±1.2	54	88	0.70±0.10	GB-OVRO	
	12.1	4.5±2.2	95	86	0.37±0.18	GB-ONS I	
	12.1	10.2±1.0	105	77	0.84±0.08	GB-ONS II	
	12.1	6.6±0.9	131	79	0.55±0.07	OVRO-ONS	
	12.1	8.7±1.3	134	87	0.72±0.11	GB-CAO	
	12.1	3.4±1.1	134	87	0.28±0.10	GB-CAO	
	12.1	2.9±0.7	174	45	0.24±0.06	OVRO-PKS	
	12.1	2.8±0.7	175	46	0.23±0.06	OVRO-PKS	
	12.1	2.7±0.7	175	46	0.22±0.06	OVRO-PKS	
	2145+06.....	4.6	3.5±1.1	37	85	0.76±0.24	GB-OVRO
4.6		4.0±1.3	47	82	0.86±0.28	GB-OVRO	
4.6		6.7±1.4	53	90	1.46±0.30	GB-OVRO	
4.6		4.0±1.3	54	85	0.86±0.28	GB-OVRO	
4.6		3.1±0.5	97	73	0.67±0.11	GB-ONS II	
4.6		3.5±0.5	100	74	0.76±0.11	GB-ONS II	
4.6		3.5±0.7	169	41	0.76±0.15	OVRO-PKS	
4.6		3.6±0.7	171	43	0.78±0.15	OVRO-PKS	
VRO 42.22.01...	6.5	4.1±1.3	49	58	0.63±0.20	GB-OVRO	
	6.5	4.7±1.0	127	89	0.72±0.15	OVRO-ONS	
	6.5	6.7±1.1	132	77	1.03±0.17	GB-CAO	
	6.5	2.1±1.3	49	58	0.47±0.29	GB-OVRO	
3C 446.....	4.5	1.4±0.7	171	46	0.31±0.16	OVRO-PKS	
	4.5	1.6±0.7	173	46	0.36±0.16	OVRO-PKS	
	4.5	1.6±0.7	173	46	0.36±0.16	OVRO-PKS	
3C 454.3.....	18.0	17.0±1.8	20	37	0.94±0.10	GB-OVRO	
	18.0	14.1±1.7	27	55	0.78±0.09	GB-OVRO	
	18.0	12.9±1.5	35	109	0.72±0.08	GB-OVRO	
	18.0	10.4±1.5	51	81	0.58±0.08	GB-OVRO	
	18.0	13.9±1.8	54	86	0.76±0.10	GB-OVRO	
	18.0	15.5±1.1	55	85	0.86±0.06	GB-OVRO	
	18.0	14.2±1.8	55	85	0.79±0.12	GB-OVRO	
	22.0	18.8±2.7	70	88	0.85±0.12	GB-ONS I	
	22.0	17.8±2.3	100	76	0.81±0.10	GB-ONS I	
	22.0	17.7±1.7	105	78	0.80±0.08	GB-ONS II	
	15.0	5.5±1.0	121	24	0.37±0.07	GB-CAO	
	15.0	6.8±1.0	131	90	0.45±0.07	GB-CAO	
	15.0	5.3±1.0	132	89	0.35±0.07	GB-CAO	
	18.0	6.5±0.9	168	33	0.36±0.05	OVRO-PKS	
	18.0	6.6±0.9	169	34	0.37±0.05	OVRO-PKS	
	18.0	5.4±0.9	171	35	0.30±0.05	OVRO-PKS	
	18.0	5.7±0.9	175	40	0.32±0.05	OVRO-PKS	
	2345-16.....	3.1	2.5±0.7	169	48	0.81±0.22	OVRO-PKS
		3.1	2.5±0.7	170	48	0.81±0.22	OVRO-PKS

be thought that the detection of fringes in these cases is not significant. This is not the case since the quoted fringe amplitudes are based on the integration of the power spectrum over the maximum frequency spread expected from local oscillator instability (Clark *et al.* 1968a). Sometimes, during periods of unusually good oscillator stability, the peak of the power spectrum clearly stands out above the noise, even though the integrated value appears to be barely significant. All of the sources listed in Tables 2 and 3 were selected with the requirement that the peak amplitude exceed the noise at the 95 percent confidence level.

It is important to note that an uncertainty in fringe visibility is equivalent to a reduction in resolving power. For example, on the Owens Valley-Parkes baseline, a measured fringe visibility of unity with a 5 percent error implies a Gaussian half-power width less than $0''.00015$. If the error is 20 percent, the size limit becomes $0''.0003$; and for 50 percent error, $0''.0005$. Thus, an increase in precision from 20 percent to 5 percent gives an improved resolution equivalent to doubling the length of the baseline.

IV. SOURCE STRUCTURE

A brief description of the small-scale structure of each source is given below. It is based not only on the data given in Tables 2 and 3 but also on previously published interferometer observations (shown in Table 4), as well as observations of interplanetary scintillations at 70 cm (Harris and Hardebeck 1969).

PKS 0019-00. The source is unresolved at 18 cm ($\lesssim 0''.025$). The 50-cm^b observations¹ give $\theta = 0''.015 \pm 0''.005$. At 13 cm, $\gamma < 0.14$ so that there is no fine structure less than $\sim 0''.002$ in diameter containing more than 15 percent of the total flux.

PKS 0106+01. QSS. Most ($\gtrsim 85$ percent) of the flux density at 6 cm comes from a component which has a spectral maximum near 8 GHz and is unresolved at all spacings at 6 cm, so $\theta \lesssim 0''.0004$. About 80 percent of the flux density comes from this small component at 13 cm.

NRAO 91. The data at 18 and 50 cm are in good agreement and indicate a relatively simple source with $\theta \sim 0''.019 \pm 0''.002$. One observation at 75 cm^a does not differ significantly from the data at shorter wavelengths.

CTA 21. The 18-cm observations suggest a core-halo structure with ~ 75 percent in a halo $0''.01$ in diameter, and 25 percent in a core $\lesssim 0''.002$. The 6-cm observations show the core to be $\sim 0''.002$. A single measurement at $5 \times 10^6 \lambda$ at 50 cm^b is somewhat lower than expected from our model and may reflect the presence of another, more extended component at longer wavelengths, which is also suggested by a minimum in the spectrum near 75 cm. Neither our data at 6 and 18 cm nor the Jodrell Bank data at 11 and 21 cm show evidence of the double structure reported at 75 cm^a.

3C 84. Seyfert galaxy. The 18-cm data show about 40 percent of the total flux density

TABLE 4

PREVIOUSLY PUBLISHED INTERFEROMETER OBSERVATIONS

Authors	Wavelength (cm)
a) Broten <i>et al.</i> 1969; Clarke <i>et al.</i> 1969.....	75
b) Jauncey <i>et al.</i> 1969.....	50
c) Jauncey <i>et al.</i> (unpublished).....	50
d) Donaldson <i>et al.</i> 1969.....	21, 11, 6
e) Donaldson and Miley 1971.....	21, 11, 6
f) Kellermann <i>et al.</i> 1970.....	13

¹ For an explanation of the superior Latin indices, see Table 4.

to be completely resolved at the shortest spacings. This is presumably the 5' halo (e.g., Ryle and Wyndram 1968). Another 45 percent of the source has an angular size of $0''.02$ at 18 cm, and 15 percent is in a core which is not significantly resolved at $35 \times 10^6 \lambda$. At 6 cm the Jodrell Bank data gave an unresolved flux of 16.6 flux units (f.u.) at $2 \times 10^6 \lambda$ in 1967. The total flux density has increased by 4 f.u. during the period 1967.0–1969.0 (Kellermann and Pauliny-Toth, unpublished) so that the small core contains about 20.5 f.u. in 1969.0. Our 6-cm data indicate a minimum in the visibility function near $80 \times 10^6 \lambda$. The data between 37 and $51 \times 10^6 \lambda$ which range over 77° of position angle suggest that the core is nearly circularly symmetric. The simplest interpretation of our data is that the core is a circular disk or ring with a diameter $0''.0025$, corresponding to 2 lt-yr with $z = 0.018$ and $H = 100 \text{ km s}^{-1} \text{ Mpc}^{-1}$. The Jodrell Bank observations^d do not show any evidence of the double structure reported at 75 cm^a. The simplest interpretation of the 75-cm data suggests a component $\leq 0''.02$ which is 15 percent of the total flux density, although the scatter in the data is large. We tentatively associate this component with the one we find at 18 cm with $\theta \sim 0''.02$. Scintillation data at 178 MHz require that not more than 10 percent of the total flux be in the smaller two components at this frequency.

Figure 1 shows the spectrum of 3C 84 at the epoch 1969.0 divided into the three components based on the data described above.

NRAO 140. QSS. The source is not significantly resolved at any spacing at 6, 18, or 50 cm^b (the 50-cm total flux density given in Jauncey *et al.* 1970 is too high by 30 percent). At 13 cm^c, $\gamma = 0.47$ at $80 \times 10^6 \lambda$. The complex spectrum, with a minimum near 5 cm, suggests that there is a component $\leq 0''.002$ in diameter which contributes about one-half of the flux density at 13 cm, and is relatively stronger at shorter wavelengths. The other component is $\leq 0''.03$.

CTA 26. QSS. A significant fraction of the flux density at 6 and 13 cm^c comes from a component $\leq 0''.001$.

NRAO 150. Most of the flux density (> 70 percent) at 18 cm comes from $< 0''.015$. At 6 cm most of the flux comes from a region $\sim 0''.0013$.

3C 119. QSS. There appears to be structure on a scale of about $0''.15$ with one or more components of the order of $0''.01$ or less.

3C 120. Seyfert galaxy. This source is highly variable, so it is difficult to compare the observations made over a period of time at different baselines. There is certainly fine

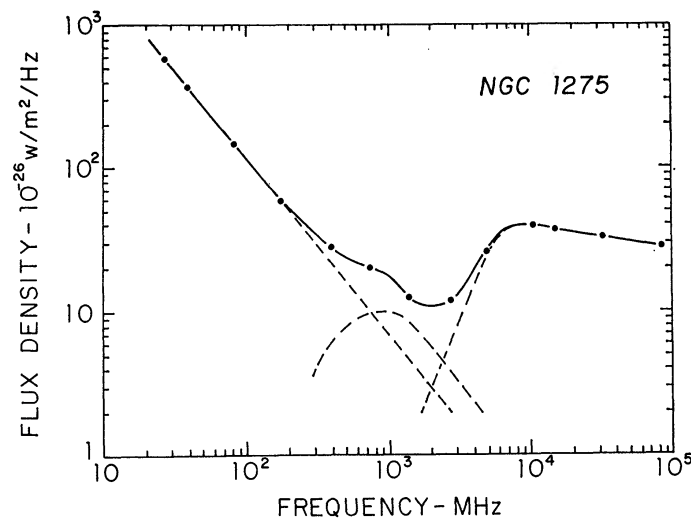


FIG. 1.—Radio spectrum of NGC 1275 (3C 84) showing the separation into separate spectral components.

structure at all wavelengths between 6 and 75 cm. At the time of the 1969 January 6-cm observations between Green Bank and Sweden, the flux density was near a maximum at 6 cm. The total amplitude of this particular outburst appears to have been at least 5 flux units, whereas the fringe amplitude was only 1.7 flux units, so that it is significantly resolved at $104 \times 10^6 \lambda$, and the size of the variable component may be estimated to have been $\geq 0''.001$.

PKS 0420-01. QSS. The observations indicate that most of the radiation at 6 cm originates in a component which is $\leq 0''.0007$.

3C 138. QSS. Donaldson and Miley (1971) find 3C 138 to be double at 11 cm with a component separation near $0''.4^e$. Our single detection requires that at least one component have structure on a scale $0''.07$ or less; similar conclusions are reached from a single measurement at 75 cm^a.

NRAO 190. The data suggest an overall size of about $0''.01$, but with one-half or more of the flux density at 6 and 13' cm coming from a component $\leq 0''.001$.

3C 147. This source does not appear to possess symmetry about either the position angle of 55° suggested by Anderson and Donaldson (1967) or the angle of 85° suggested by the 75-cm data^a. It is clear that in both position angles there is structure at least as large as $0''.07$ as well as appreciable structure smaller than $0''.02$.

PKS 0605-08. The source is unresolved at 6 cm at $100 \times 10^6 \lambda$. At 13 cm^f, $\gamma \sim 0.6$ at $80 \times 10^6 \lambda$. This suggests that most of the flux density at 6 cm comes from $\leq 0''.0007$, and that at 13 cm this component contributes only about 60 percent to the total flux density.

PKS 0607-15. At least 30 percent of the flux density at 6 and 13 cm^f comes from a region $\leq 0''.002$.

DW 0742+10. The source may be partially resolved at 18 and 6 cm. The complex spectrum suggests two components, with the smaller one being $\leq 0''.001$ and at least 2.4 f.u. at 6 cm and only 0.8 f.u. at 13 cm^f. The overall size appears to be about $0''.01$.

PKS 0834-20. The limited data suggest that most of the emission at 18 cm comes from a region $\sim 0''.01$.

4C 39.25. QSS. There is an unresolved component at 6 cm which is $\leq 0''.0004$. Its flux density is about 6.5, 2.5, and 1.5 f.u. at 6, 13', and 18 cm, respectively. In addition, there is a more extended component at 18 cm which is $\geq 0''.02$. The spectrum has a rather deep minimum near 30 cm.

PKS 1055+01. QSS. There appear to be at least two small components, one which contributes 60-70 percent of the total flux density at 50^c and 75 cm^a and is in the range $0''.001-0''.01$, and a second which is unresolved at 6 and 13 cm^f and is $\leq 0''.0005$ and contributes about 50 percent of the total flux density at these wavelengths.

PKS 1121-14. QSS. The data indicate at least two or three distinct components. One, which is stronger at long wavelengths, is $\sim 0''.003$. The second is $\leq 0''.001$ and is 15 percent of the total at 13 cm^f. It appears to be well resolved at 6 cm at $170 \times 10^6 \lambda$, where it contributes most of the observed flux density.

PKS 1148-00. QSS. The data at 18 and 13 cm^f are in only fair agreement. The simplest model is a source $\sim 0''.002$, but the 18-cm points are somewhat low on this model; alternatively, there may be an unresolved core $\leq 0''.002$.

3C 273. QSS. Both the 6- and 18-cm visibility curves suggest classical core-halo structure (Figs. 2a and 2b). The 18-cm data show that there is a halo (component B) of $0''.022$ which contributes ~ 50 percent (15 f.u.) of the total flux density at this wavelength, exclusive of component A. The second component (C), also 15 f.u., is barely resolved at 18 cm. At 6 cm this component contributes about 60 percent of the total flux (20 f.u.); it is completely resolved and is $\sim 0''.002$. A third component (D) has about 20 percent of the total flux (6 f.u.) and appears to be unresolved at $175 \times 10^6 \lambda$, so it is $\leq 0''.0004$.

The absence of a significant minimum in the visibility function at 6 cm suggests that

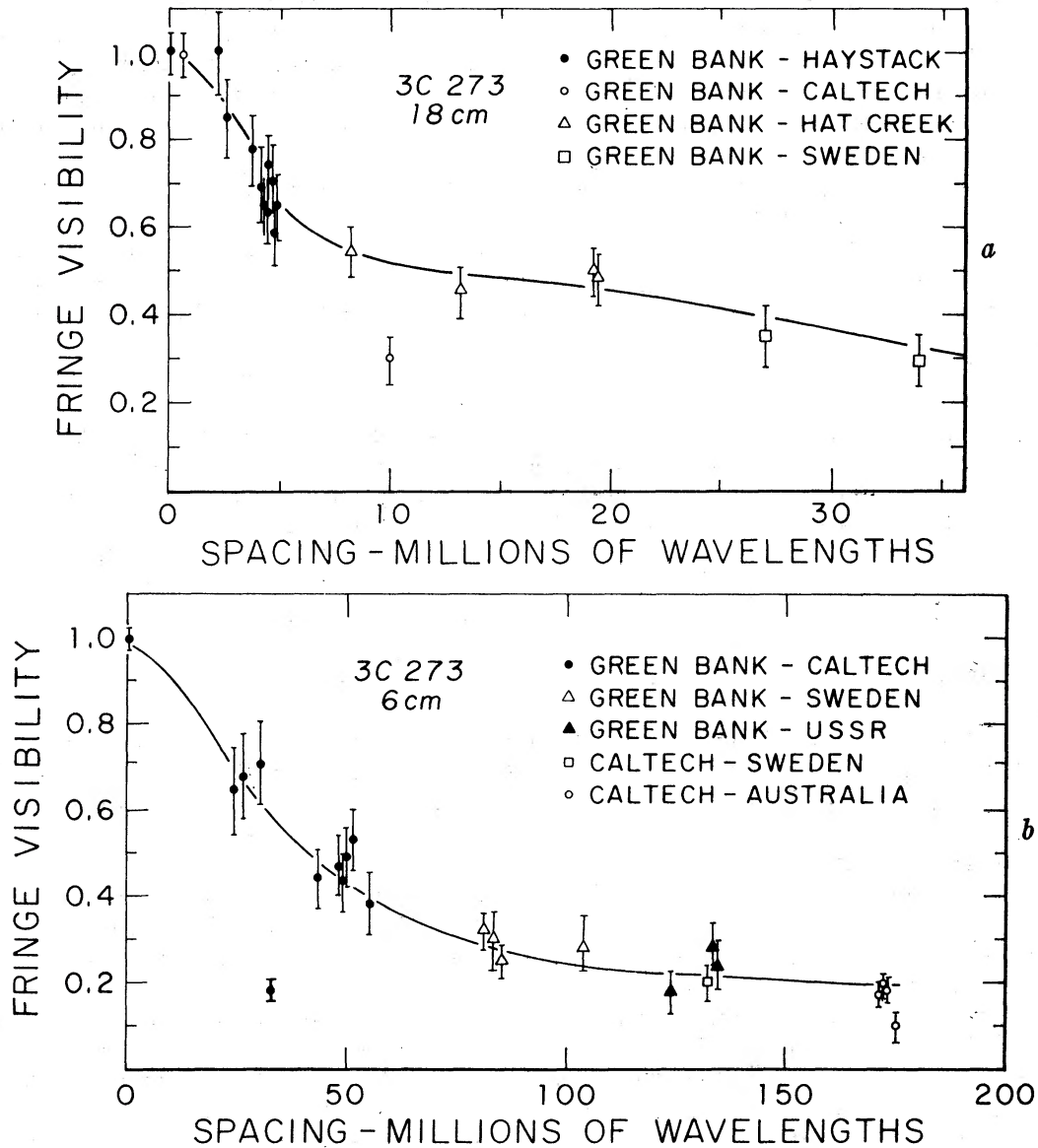


FIG. 2a.—Visibility function of the compact source in 3C 273 at 18 cm.

FIG. 2b.—Visibility function of the compact source in 3C 273 at 6 cm.

components C and D are not separated by more than the size of component C ($\sim 0''.002$). The absence of a clear minimum near $5 \times 10^6 \lambda$ at 18 cm similarly suggests that components B and C are not separated by more than $0''.02$. There is one very low point at $10 \times 10^6 \lambda$ at 18 cm. This may be due to component separation of about $0''.01$, but it may also be due to observational error. Clearly, more extensive measurements are necessary to determine the extent to which components B, C, and D are coincident.²

The single measurement at 2.8 cm at 280×10^6 wavelengths suggests that component D is partially resolved and is about $0''.0004$ in diameter (Broderick *et al.* 1970*a, b*);

² Note added 1971 July 29.—More recent measurements at 3.8 cm indicate that component C is double with a separation of $0''.00155$ (Cohen *et al.* 1971, *Ap. J.* [in press]).

but this result is very uncertain, and further high-resolution measurements are needed.

At 13 cm^f at $80 \times 10^6 \lambda$, components B and C are nearly fully resolved and the single measurement gives the flux density of component D as 1.9 f.u. At 50 cm^e at $4.6 \times 10^6 \lambda$, component A is completely resolved, and the main contribution to the fringe amplitude comes from component B which is partially resolved at this spacing. The estimated total flux density of component B at 50 cm based on the angular size measured at 18 cm is about 25 f.u., which is consistent with the spectrum shown in Figure 3. It is not clear how the complex model proposed by the Canadian observers from their 75-cm observations^a relates to our model.

3C 279. QSS. It is well known that 3C 279 contains two major components, one of which is small and predominates at short wavelengths. Our data suggest that this compact component contains three subcomponents. The 18-cm and 6-cm visibility curves suggest core-halo structure at both wavelengths. At 18 cm ~ 20 percent (2 f.u.) of the total flux is in an extended component (A), 30 percent (3.5 f.u.) in a component B $\sim 0''.022$, and 50 percent (5.5 f.u.) in an unresolved component (C). At 6 cm component C is about 60 percent of the total (10 f.u.), is resolved, and is $\sim 0''.001$. Component D, which contributes about 15 percent of the total (4.5 f.u.), is unresolved and is $\leq 0''.0004$. At 13 cm^f component B must be completely resolved at $80 \times 10^6 \lambda$. If component C is $\sim 0''.001$, then its visibility at 13 cm is about 0.6. The measured fringe amplitude is 3.2 f.u., and so component D must be about 2 f.u. at 13 cm. At 75 cm, component A is completely resolved and C and D contribute negligible flux density, so the observations at 75 cm^a must refer to component B which contributes 35 percent (4.5 f.u.) at this frequency. Interplanetary scintillation (IPS) observations made close to the Sun at 11 cm (Cohen and Gundermann 1969) have shown a component $\leq 0''.002$; this must be components C and D. The size quoted by the Canadian observers ($0''.010 \pm 0''.003$) at P.A. 90° does not agree too well with our size of $0''.022$ at P.A. 65° , so component B may be elongated.

PKS 1245-19. The source is unresolved at 18 cm at $1.4 \times 10^6 \lambda$ and completely resolved at 13 cm^f at $80 \times 10^6 \lambda$, so $0''.002 \leq \theta \leq 0''.04$.

3C 287. QSS. At 18 cm one-half of the source is unresolved at $4.7 \times 10^6 \lambda$. The source is completely resolved at 13 cm at $80 \times 10^6 \lambda$, so there must be a component $0''.002 \leq \theta \leq 0''.01$. At 50 cm^e this component appears to contribute only about 15 percent of the

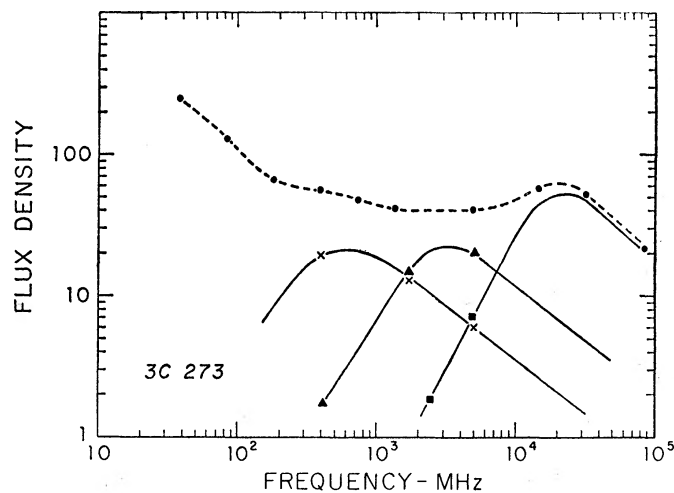


FIG. 3.—Radio spectrum of the compact source in 3C 273 showing the separation into separate components. X, Component B; ▲, Component C; ■, Component D.

total flux density. At 70 cm the IPS index $m = 0.8$, so that the larger component is also rather compact, probably with a diameter near $0''.03$. The 75-cm interferometer data^a, however, indicate double structure on a scale of $0''.1-0''.2$.

3C 286. QSS. Our data at 18 cm are consistent with a circularly symmetric source of diameter $\sim 0''.03$. A single measurement at 50 cm^c is also consistent with this. The more extensive data at 75 cm^a imply considerably more complex structure on a scale greater than $\sim 0''.1$, although this may refer to another component which contributes at longer wavelengths. The presence of this low-frequency component is suggested also from the spectrum which does not show the low-frequency cutoff expected of the $0''.03$ component. At 70 cm, the IPS index $m = 0.6$, which suggests that the low-frequency component contains about 40 percent of the flux at this wavelength. No fringes were seen at 13 cm^f, so there is no fine structure less than $\sim 0''.002$.

3C 309.1. QSS. There is no evidence of self-absorption in a small component in the overall spectrum, which is close to a power law. The 18-cm data show that the source is unresolved at $4.3 \times 10^6 \lambda$ and is $\leq 0''.015$. At 75 cm^a there are at least two components.

DA 406. QSS. The source is unresolved at 6 cm at $100 \times 10^6 \lambda$ and is less than $0''.0008$. About 50 percent of the flux density is in this small component at 13 cm^f (1.6 f.u.) and at 18 cm (1.6 f.u.).

PKS 1510-08. QSS. Most of the source at 6 cm is $\leq 0''.0004$. At 13 cm^f only 40 percent of the source is in this unresolved component. A comparable fraction is in a component $\leq 0''.01$ at 75 cm^a.

4C 05.64. At 6, 13, and 18 cm at least 40 percent of the flux comes from a component less than $\sim 0''.001$. The source is unresolved at 50 cm^c at $5 \times 10^6 \lambda$, so all of the source is less than $\sim 0''.015$ at this wavelength.

DW 1555+00. The source is not resolved by any of our measurements. Most of the source is $\leq 0''.01$ at 50 cm^c, $\leq 0''.0006$ at 13 cm^f, and $\leq 0''.0004$ at 6 cm.

CTD 93. Galaxy. The major component is approximately $0''.0025$, but the high visibility observed at 13 cm^f at 80×10^6 compared with that observed at $35 \times 10^6 \lambda$ at 18 cm suggests possible structure $\leq 0''.002$.

3C 345. QSS. About 60 percent (4 f.u.) of the total flux density is in an unresolved component $\leq 0''.0007$ at 6 cm. At 13 cm^f the flux density of this component is 2.5 f.u., and at 18 cm it is 1.6 f.u. In addition, there is a larger component $\sim 0''.005$ which is nearly completely resolved at $35 \times 10^6 \lambda$ at 18 cm and contributes half of the total flux density at 75 cm^a. The remainder of the source at 75 cm^a is in a more extended component $\geq 0''.05$, which does not contribute more than 20 percent of the total at 18 cm.

NRAO 530. There is a component which contains about 50 percent (2.0 f.u.) of the flux density at 6 cm and is less than $\sim 0''.002$. At 13 cm^f this component is much weaker and is only ~ 0.4 f.u. At 18 cm this component has a negligible contribution and most of the flux density comes from a region $\sim 0''.005$. A considerably larger size of about $0''.03$ is found at 75 cm^a.

3C 380. QSS. There is a component which is $\leq 0''.002$ and contributes about 30 percent of the total flux density at 6 or 18 cm (2.5 and 3.5 f.u., respectively). The 75-cm^a data apparently refer to a more extended component.

3C 418. At least 70 percent of the flux density at 18 cm is in an unresolved component less than $\sim 0''.015$.

PKS 2127+04. The source is unresolved at 50 cm^b and is less than $\sim 0''.015$. The 13-cm^f data give $\theta \sim 0''.002$, but the fringe amplitude observed at 18 cm at 15×10^6 is too low for a source this small, and may indicate more complex structure. Most of the flux comes from a component which has a sharp cutoff below 1 GHz.

PKS 2134+004. QSS. The 6-cm data indicate a diameter of $0''.0008$, but the large scatter suggests possible complex structure. The 13-cm^f point fits better to a source about twice this size, but at this wavelength there may be more extended structure as

suggested by a slight positive curvature of the spectrum. Most of the flux at centimeter wavelengths comes from a component which has a sharp cutoff near 6 cm.

PKS 2145+06. QSS. The source is essentially unresolved at 6 cm, so most of the flux is from a component of about 4 f.u. and less than $\sim 0''.0004$. This component contributes about 2 f.u. at 13 cm^f and at 18 cm. At 50 cm^b the source is probably unresolved at $5 \times 10^6 \lambda$, so the entire source is less than $\sim 0''.015$.

VRO 42.22.01 (BL Lac). QSS? The source is unresolved at 6 cm and is less than $\sim 0''.0004$. At 13 cm^f this small component is only 22 percent (1.3 f.u.) of the total flux.

PKS 2203-18. QSS. $\theta \sim 0''.05$.

CTA 102. QSS. The interferometer data indicate more complex structure than suggested by the relatively simple spectrum. At 18 cm about 50 percent of the flux comes from a halo $\sim 0''.007$, and 50 percent is unresolved and is less than $\sim 0''.003$. The 13-cm^f measurement requires that at least 20 percent of the flux at 13 cm be in a component $\leq 0''.001$. The 75-cm^a data suggest the presence of a larger component containing 15 percent of the flux, and having a size greater than $\sim 0''.2$. There is no evidence of this larger component in our 50-cm data^b nor in the IPS data at 70 cm, which give an index $m = 1$. However, the uncertainties in the 50-cm interferometer data and the IPS data are sufficiently large that there is no real inconsistency.

3C 446. QSS. There is a component of about 2 f.u. which is unresolved at 6 cm between 50 and $170 \times 10^6 \lambda$. It is less than $\sim 0''.0004$, and is 1 f.u. at 13 cm^f. At 18 cm there is a second small component which has structure at 18 cm on a scale $\sim 0''.02$.

3C 454.3. QSS. The interpretation of the 6-cm data is difficult due to the large decrease in total flux density which occurred in 1969. There is a component of about 5 f.u. at 6 cm which is unresolved at $175 \times 10^6 \lambda$ and is less than $\sim 0''.0004$. Most of the rest of the flux at 6 cm comes from a component which is resolved by $100 \times 10^6 \lambda$ and is $\sim 0''.002$. This component is also resolved at 18 cm where it contributes most of the flux, and the 13-cm^f data suggest possible complex structure. The entire source is unresolved by us at 50 cm^b and is less than $\sim 0''.15$. The 75-cm interferometer data^a suggest structure on a scale of 1" or greater, but the observed scintillation index of unity suggests that nearly the entire source be contained within $0''.2$ at 70 cm.

PKS 2345-16. Complex spectrum; QSS. The source is essentially unresolved at 13^f and 6 cm, so $\theta < 0''.0004$.

The models used to describe the sources are only a first approximation to the true structure in the sense that we have always taken the simplest model which is consistent with our data. In particular, we have not forced our models to include every data point, but believing that our estimated errors are true standard deviations, we have allowed up to 30 percent of our points to differ from the model by more than the quoted error. For example, when the fringe visibility at only one out of four or five measured spacings is low, we have not interpreted this as evidence of double structure. Rather, we consider it more likely to be due to a statistical fluctuation, or to loss of coherence for some other reason. This means, however, that our analysis is biased against finding any double or other multiple structure which may exist.

Often when there is only a small range of spacings covered by the data, it is difficult to choose between a model consisting of a partially resolved simple Gaussian source and one consisting of a completely resolved component plus a completely unresolved component. To choose between these two cases we have considered the spectrum of the source. If the spectrum is simple and contains only a single maximum, we consider it likely that the structure is also simple; but if the spectrum is complex and shows one or more maxima or minima in the frequency range discussed, then we have assumed that this is due to several components which become opaque at different wavelengths. In a number of cases, however, such as 3C 84, 3C 273, and 3C 279, where there are reasonably

extensive interferometer data at several wavelengths, it is clear from the fringe visibilities alone that there must be up to three or more distinct components.

V. VARIABLE SOURCES

The unambiguous resolution of variable source components would permit a direct test of the expanding source model (Shklovskii 1965) and allow the rate of expansion to be determined. It would also be possible to calculate the rate of change of the magnetic field strength and, in the case of identified sources whose distance is known, the total energy content. Also, for the identified variable sources it would be possible to test the hypothesis that the apparent expansion velocity is greater than that given by the usual light-travel-time arguments (e.g., Rees 1968). Most of the variable sources are, however, too small to be resolved with the baselines used in the measurements reported here.

One exception is the relatively nearby radio galaxy NGC 1275 (3C 84). 3C 84 was resolved on the Green Bank–Onsala baseline in both the 1968 and 1969 measurements. The fringe visibility appears to have significantly decreased during the one year between the two sets of observations, indicating an increase in angular size during this time. It is, however, difficult to be quantitative since the uncertainty in the visibility in 1968 is large and because the low values of γ cause the calculations to be strongly model dependent. If we interpret our 1969 observations as indicating a circular disk structure (see § V), then the diameter was $0''.0025 \pm 0''.0002$ in 1969.0 and $0''.0017 \pm 0''.0002$ in 1968.0. The later value is greater than the value of $0''.001$ given by Kellermann *et al.* (1969), because the results in that paper were based on a circular Gaussian model rather than the circular disk required by the new data. If we assume that $z = 0.018$ and $H = 100 \text{ km s}^{-1} \text{ Mpc}^{-1}$, then the distance to NGC 1275 is 78 Mpc and the corresponding diameters are 2.1 ± 0.2 and $1.4 \pm 0.2 \text{ lt-yr}$ in 1969.0 and 1968.0, respectively, so the diameter has increased by $0.7 \pm 0.3 \text{ lt-yr}$ in one year, giving an expansion velocity $v/c = 0.35 \pm 0.15$. This is greater than estimated previously (Kellermann *et al.* 1968), implying that the variable component is much younger than the ten years which was previously assumed from an analysis of the radio intensity variations. Further measurements are clearly required to confirm the observed size variation and to determine more accurately the expansion rate.

The direct resolution of a variable component has also been reported for 3C 273 (Gubbay *et al.* 1969) and for 3C 279 (Moffet *et al.* 1971). In the case of 3C 279, their 13-cm observations, which are spaced over a two-year period, suggest that the expansion is relativistic with $\gamma = (1 - v^2/c^2)^{-1/2} \gtrsim 2$. Similar data for 3C 273 show the existence of an unresolved component which does not vary in intensity, while the flux of a larger resolved component was decreasing. This is an interesting and surprising result, since it means that the observed variations in flux density do not necessarily occur in the smallest component, as might have been expected.

This suggests to us a small, well contained, but highly energetic core, which occasionally releases a cloud of relativistic particles which then expands and rapidly becomes bigger than the core.

The only other variable source for which there is a relevant observation is 3C 454.3, which showed a decrease in total flux density from 22 to 15 f.u. between the time of the Green Bank–Onsala observations in 1969 January and the Green Bank–Crimea observations in 1969 October. This is reflected by a comparable drop in fringe amplitude expected if the variable component is unresolved at $100 \times 10^6 \lambda$.

VI. DISCUSSION

Since our observations cover only very limited regions of the (u, v) -plane, it has been difficult to determine in detail the structure of individual sources, particularly for the weaker sources where the uncertainties in fringe visibilities are large. Moreover, many of

the sources are variable, a condition which further limits the interpretation of the data. We believe, however, that our data determine (1) the overall size of the compact radio sources, (2) the approximate scale of individual components, and (3) the general dependence of the structure on wavelength.

It is apparent from the present data, and from previously published work at lower resolution, that there is a continuous range of scale in extragalactic sources down to angular dimensions of $0''.0004$ or less. If the quasi-stellar sources are assumed to be at cosmological distances, then the typical linear dimensions of the smallest components are of the order of a few parsecs or less. The unresolved component in 3C 273 is smaller than 1 pc.

The observed peak brightness temperatures range up to a value of about 10^{12} °K, which is the limiting brightness temperature that can occur in an opaque incoherent synchrotron source (Kellermann and Pauliny-Toth 1969). We note in passing that such high measured brightness temperatures preclude any possibility that the observed radio emission in sources with peaked or complex spectra is due to any thermal process. Using the synchrotron model to interpret the measured angular size and cutoff frequency we estimate the magnetic field strengths, in the usual way, to be in the vicinity of 10^{-4} gauss in most of the resolved opaque components.

In general, when a source has been observed at several wavelengths at comparable spacings, the fringe visibility is greater at the shorter wavelengths. Figure 4 shows a plot of the fringe visibility at 6 cm measured near $80 \text{ million } \lambda$, or interpolated from data

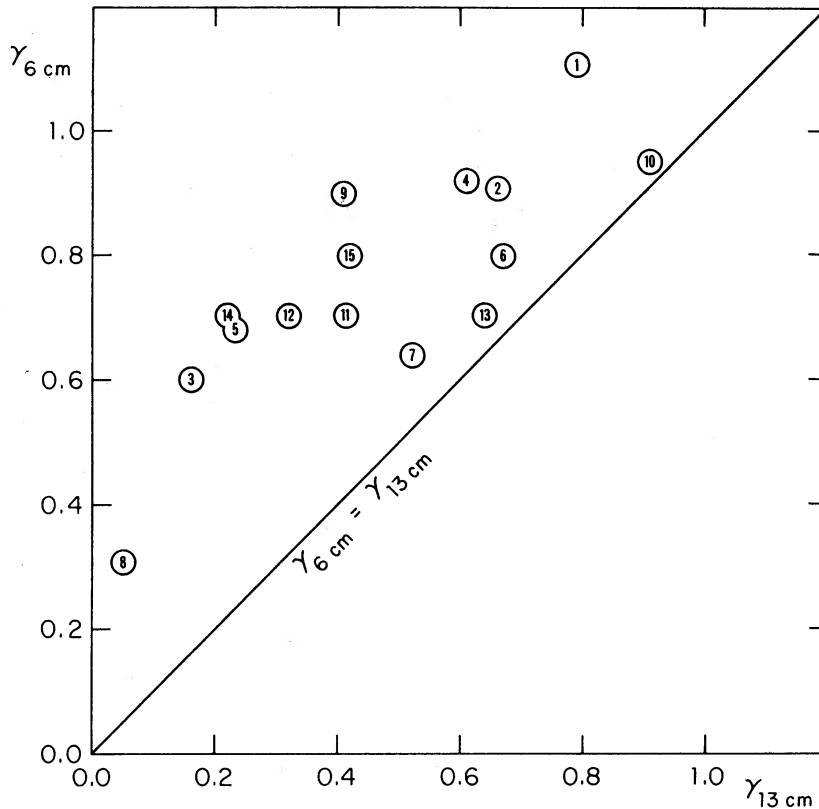


FIG. 4.—Fringe visibility at 6 cm vs fringe visibility at 13 cm for a spacing of $80 \times 10^6 \lambda$. Numbers refer to the following sources: (1) 0106+01; (2) CTA 26; (3) 3C 120; (4) 0605-08; (5) 0742+10; (6) 4C 39.25; (7) 1055+01; (8) 3C 273; (9) 1510-08; (10) 1555+00; (11) 3C 345; (12) 2134+00; (13) 2145+06; (14) VRO 42.22.01; (15) 3C 454.3.

near 50 and 100 million λ , versus the fringe visibility at 80 million λ measured at 13 cm (Kellermann *et al.* 1970). The visibility measured at 6 cm is in every case greater than that measured at 13 cm. This shows directly that the apparent angular dimensions are smaller at the shorter wavelengths, so the compact sources in general do not contain a single opaque component whose size is independent of wavelength.

The apparent variation of size with wavelength could be due to the presence of several components which become optically thick at different wavelengths, as suggested by the shape of the radio spectra (e.g., Kellermann and Pauliny-Toth 1969; Jauncey *et al.* 1970) or to the effect of interstellar scattering (e.g., Harris, Zeissig, and Lovelace 1970). For the following reasons, we believe that our data are not significantly affected by interstellar scattering and that the results are most simply interpreted as due to the higher self-absorption cutoff frequency in the smaller components.

1. The expected scattering size at 13 cm ($\sim 10^{-4}$ arc sec) is an order of magnitude less than the smallest source capable of being resolved on a baseline of $80 \times 10^6 \lambda$ ($\sim 10^{-3}$ arc seconds).

2. The measured angular dimensions are generally close to what is expected from self-absorption with magnetic fields of the order of 10^{-4} gauss.

3. The measured peak brightness temperatures are of the order of 10^{12} ° K at all wavelengths, as expected from self-absorption and inverse Compton cooling.

4. Sources with complex radio spectra tend to show frequency-dependent angular structure, while the size of sources with relatively simple spectra (a single maximum and sharp low-frequency cutoff) generally are independent of wavelength.

5. In several sources (e.g., 3C 273) where there is sufficient interferometer data, the fringe-visibility diagrams show directly the presence of several components, with the larger components being stronger at the longer wavelengths.

In the range of angular dimensions from $0''.0005$ to $0''.05$ where our results are most sensitive, there is no clear evidence in our data that the components are spatially separated. However, because we have considered only those observations which gave fringes and because we place little weight on the few cases where there are isolated low fringe visibilities, we have systematically discriminated against detecting multiple structure. There is, however, evidence from the observations made at 75 cm (Clarke *et al.* 1969) of component separations in the range $0''.01$ – $0''.1$. Clearly measurements with more coverage of the (u, v) -plane are required before more detailed models of source structure can be pursued.

A total of twelve sources gave fringes on the longest baseline, $176 \times 10^6 \lambda$, between California and Australia. These sources all contain significant structure on a scale of $0''.0005$. Several sources including 0106+01, 3C 273, 3C 279, 1555+00, 2145+06, 3C 345, 3C 454.3, and 2345–16 have unresolved components which are $0''.0004$ or less in extent, and observations at higher resolution are necessary to study them.

Longer baselines are impractical due to restricted common sky coverage from locations near diametrical positions on the Earth, so that the observations must be extended to shorter wavelengths.

We have reported observations at 2.8 cm made between Green Bank and the Crimea, a baseline separation of $280 \times 10^6 \lambda$ (Broderick *et al.* 1970*a, b*). However, the lower sensitivity of the receivers, together with decreased local oscillator stability, allowed only weak fringes to be seen on two sources, 4C 39.25 and 3C 273. Little or no increase in the effective resolution was achieved because of the large uncertainty in fringe visibility.

It is interesting to note that all of the stronger sources should be resolved by using baselines restricted to the surface of the Earth, because a source with 1 f.u. or more of unresolved flux at this baseline (irrespective of the frequency of observation) would have a brightness temperature in excess of the limit set by inverse Compton cooling of 10^{12} ° K (Kellermann and Pauliny-Toth 1969). This follows from the fact that for a

constant peak brightness temperature, $T_p = \frac{1}{2}\lambda^2 S/k\theta^2$, and peak flux density S , the angular size θ of an opaque synchrotron source is directly proportional to the wavelength of maximum flux density. Thus, if on a given physical baseline D the effective resolution is given by $\theta \simeq \lambda/3D$, and if $T_p \leq 10^{12}$ °K, then for all sources with $S_p \geq 3$ f.u. the maximum required baseline D is 10000 km if the observations are made at the wavelength of maximum flux density. At shorter wavelengths, sources well under 1 f.u. may be resolved with terrestrial baselines, so that there seems to be little need to use baselines in space or between the Earth and the Moon.

This conclusion does not apply to sources such as molecular masers or pulsars, which do not radiate by an incoherent synchrotron mechanism, and are not therefore limited to 10^{12} °K. In the case of the known pulsars, however, they radiate most strongly at wavelengths where interstellar "seeing" is likely to limit the maximum usable baselines to less than one Earth diameter (e.g., Harris *et al.* 1970).

We are grateful to the many people who have contributed in various ways to the success of these observations. These include S. Weinreb, W. Vrable, M. Balister, and J. Payne at NRAO; A. Moffet and G. Seielstad at OVRO; L. Kogan and V. Kostenko, of the Institute for Space Research; V. Efanov and others at the Crimean Astrophysical Observatory; and B. Höglund, B. Hansson, E. Kollberg, and others at Onsala.

We are thankful to P. O. Lundbom and C. Åbom of the Swedish Research Institute for National Defense whose aid and cooperation allowed us to synchronize our clock in Stockholm for the observations in Sweden and the U.S.S.R. Similar assistance was given to us by the staffs of the Jet Propulsion Laboratory, the Timing Section at Point Mugu, and the NASA DSN Tidbinbilla Tracking Station. We also wish to thank Y. Pariskii and others at the Pulkova Observatory for their generous assistance in transferring the time between Stockholm and Crimea.

Many of the tapes were processed by T. Clark at the Goddard Space Flight Center, and we are grateful to him and his staff for their generous help. We are also grateful to the Goddard Space Flight Center for the loan of their hydrogen maser and to Dr. H. Peters for his continued interest and aid in the operation of the maser.

The recording system used in these experiments was developed by C. Bare before his unfortunate death, and we wish to acknowledge his extensive contribution.

These experiments would not have been possible without the effort and cooperation of J. G. Bolton, D. S. Heeschen, W. E. Howard III, A. Severny, I. Shklovskii, and G. Stanley.

Part of this work was done while one of us (K. I. K.) was on leave of absence from NRAO at the California Institute of Technology. One of us (D. B. S.) was supported by a NSF predoctoral fellowship.

REFERENCES

- Anderson, B., and Donaldson, W. 1967, *M.N.R.A.S.*, **137**, 81.
 Bare, C., Clark, B. G., Kellermann, K. I., Cohen, M. H., and Jauncey, D. L. 1967, *Science*, **157**, 19.
 Broderick, J. J., Vitkevitch, V. V., Jauncey, J. L., Efanov, V. A., Kellermann, K. I., Clark, B. G., Kogan, L. R., Kostenko, V. I., Cohen, M. H., Matveyenko, L. I., Moiseyev, I. G., Payne, J. G., and Hansson, B. 1970a, *Astr. Zh.*, **47**, 784.
 ———. 1970b, *Radio Science*, **5**, 1281.
 Broten, N. W., Clarke, R. W., Legg, T. H., Locke, J. L., Galt, J. A., Yen, J. L., and Chisholm, R. M. 1969, *M.N.R.A.S.*, **146**, 313.
 Clark, B. G., Kellermann, K. I., Bare, C. C., Cohen, M. H., and Jauncey, D. L. 1968a, *Ap. J. (Letters)*, **153**, L67.
 ———. 1968b, *Ap. J.*, **153**, 705.
 Clarke, R. W., Broten, N. W., Legg, T. H., Locke, J. L., and Yen, J. L. 1969, *M.N.R.A.S.*, **146**, 381.
 Cohen, M. H., and Gundermann, E. J. 1969, *Ap. J.*, **155**, 645.
 Donaldson, W., and Miley, G. K. 1971 (in preparation).

- Donaldson, W., Miley, G. K., Palmer, H. P., and Smith, H. 1969, *M.N.R.A.S.*, **146**, 213.
- Gubbay, J., Legg, A. J., Robertson, D. S., Moffet, A. T., Ekers, R. D., and Seidel, B. 1969, *Nature*, **224**, 1094.
- Harris, D. E., and Hardebeck, E. G. 1969, *Ap. J. Suppl.*, **19**, 115.
- Harris, D. E., Zeissig, G. A., and Lovelace, R. V. 1970, *Astr. and Ap.*, **8**, 104.
- Jauncey, D. L., Bare, C. C., Clark, B. G., Kellermann, K. I., and Cohen, M. H. 1970, *Ap. J.*, **160**, 337.
- Kellermann, K. I., Clark, B. G., Bare, C. C., Rydbeck, O., Elder, J., Hansson, B., Kollberg, E., Höglund, B., Cohen, M. H., and Jauncey, D. L. 1968, *Ap. J. (Letters)*, **153**, L209.
- Kellermann, K. I., Clark, B. G., Jauncey, D. L., Cohen, M. H., Shaffer, D. B., Moffet, A. T., and Gulkis, S. 1970, *Ap. J.*, **161**, 803.
- Kellermann, K. I., and Pauliny-Toth, I. I. K. 1969, *Ap. J. (Letters)*, **155**, L71.
- Moffet, A. T., Gubbay, J., Robertson, D. S., and Legg, T. H. 1971, *Proc. IAU Symp. No. 44* (in press).
- Rees, M. J. 1968, *Nature*, **211**, 468.
- Rees, M. J., and Simon, M. 1968, *Ap. J. (Letters)*, **152**, L145.
- Ryle, M., and Windram, M. D. 1968, *M.N.R.A.S.*, **125**, 1.
- Shklovskii, J. 1965, *Astr. Zh.*, **42**, 30 (English transl. in *Soviet Astr.—AJ*, **9**, 22).